

The fractional a.c. Josephson effect in a semiconductor–superconductor nanowire as a signature of Majorana particles

Leonid P. Rokhinson^{1*}, Xinyu Liu² and Jacek K. Furdyna²

Topological superconductors that support Majorana fermions have been predicted when one-dimensional semiconducting wires are coupled to a superconductor^{1–3}. Such excitations are expected to exhibit non-Abelian statistics and can be used to realize quantum gates that are topologically protected from local sources of decoherence^{4,5}. Here we report the observation of the fractional a.c. Josephson effect in a hybrid semiconductor–superconductor InSb/Nb nanowire junction, a hallmark of topological matter. When the junction is irradiated with a radiofrequency f_0 in the absence of an external magnetic field, quantized voltage steps (Shapiro steps) with a height $\Delta V = hf_0/2e$ are observed, as is expected for conventional superconductor junctions, where the supercurrent is carried by charge- $2e$ Cooper pairs. At high magnetic fields the height of the first Shapiro step is doubled to hf_0/e , suggesting that the supercurrent is carried by charge- e quasiparticles. This is a unique signature of the Majorana fermions, predicted almost 80 years ago⁶.

In 1928 Dirac reconciled quantum mechanics and special relativity in a set of coupled equations that became the cornerstone of quantum mechanics⁷. Its main prediction that every elementary particle has a complex conjugate counterpart—an antiparticle—has been confirmed by numerous experiments. A decade later Majorana showed that Dirac's equation for spin-1/2 particles can be modified to permit real wavefunctions^{6,8}. The complex conjugate of a real number is the number itself, which means that such particles are their own antiparticles. Although the search for Majorana fermions among elementary particles is continuing⁹, excitations with similar properties may emerge in electronic systems⁴, and are predicted to be present in some unconventional states of matter^{10–15}.

Ordinary spin-1/2 particles or excitations carry a charge, and thus cannot be their own antiparticles. In a superconductor, however, free charges are screened, and charge-less spin-1/2 excitations become possible. The Bardeen–Cooper–Schrieffer (BCS) theory of superconductivity allows fermionic excitations that are a mixture of electron and hole creation operators, $\gamma_i = c_i^\dagger + c_i$. This creation operator is invariant with respect to charge conjugation, $c_i^\dagger \leftrightarrow c_i$. If the energy of an excitation created in this way is zero, the excitation will be a Majorana particle. However, such zero-energy modes are not permitted in ordinary s -wave superconductors.

The present work is inspired by ref. 15, where the authors show that Majorana fermions can be formed in a coupled semiconductor/superconductor system. Superconductivity can be induced in a semiconductor material by the proximity effect. At zero magnetic field electronic states are doubly degenerate and Majorana

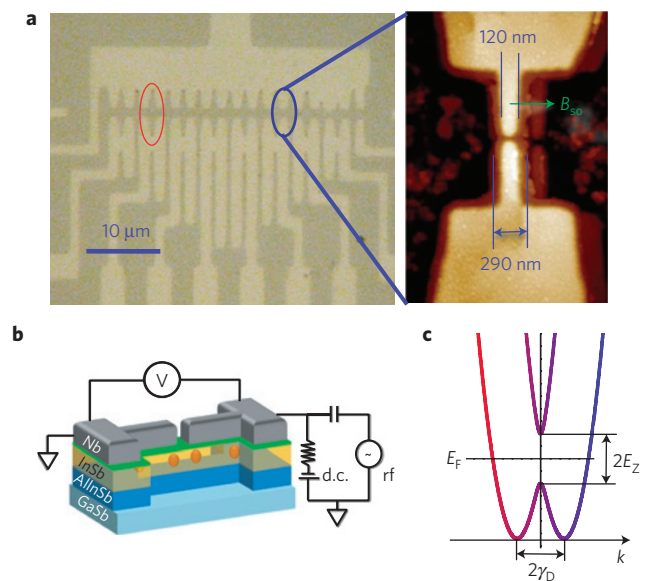


Figure 1 | Devices layout. **a**, Optical image of a sample with several devices. A single d.c. SQUID device is outlined with a red oval. On the enlarged AFM image a single Josephson junction is shown. The light areas are Nb. A light brown halo around Nb is a thin 2–3 nm Nb layer which defines the width of the semiconductor wire after wet etching. The direction of the spin-orbit field B_{so} is indicated by the green arrow. **b**, A schematic view of the device, the orange dots mark the expected positions of Majorana particles inside the InSb nanowire. **c**, Energy dispersion in a material with spin-orbit interaction γ_D in the presence of magnetic field $B \perp B_{so}$.

modes are not supported. In semiconductors with strong spin–orbit interactions the two spin branches are separated in momentum (\mathbf{k}) space, but spin–orbit interactions do not lift the Kramer's degeneracy. However, in a magnetic field $\mathbf{B} \perp \mathbf{B}_{so}$ there is a range of energies where double degeneracy is lifted¹⁶, see the schematic in Fig. 1c. If the Fermi energy E_F is tuned to be within this single-mode range of energies, $E_Z > \sqrt{\Delta^2 + E_F^2}$, (where Δ is the proximity gap, $E_Z = g\mu_B B/2$ is the Zeeman energy, μ_B is the Bohr magneton, and g is the Landé g -factor), the proximity effect from a conventional s -wave superconductor induces p -wave pairing in the semiconductor material and drives the system into a topological superconducting state which supports Majorana particles. Theoretically, it has been predicted that proper conditions for this to occur can be realized

¹Department of Physics, Birck Nanotechnology Center and School of Electrical and Computer Engineering, Purdue University, West Lafayette, Indiana 47907, USA, ²Department of Physics, University of Notre Dame, Notre Dame, Indiana 46556, USA. *e-mail: leonid@purdue.edu.

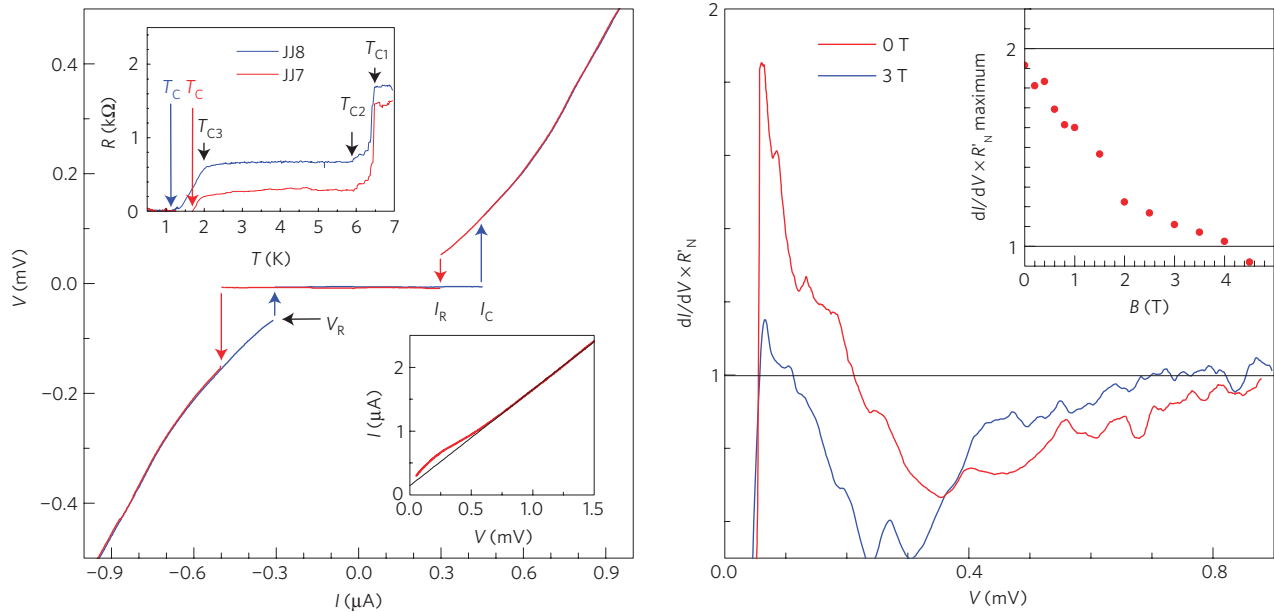


Figure 2 | Characterization of Josephson junctions. Left: $V(I)$ characteristic of a Nb/InSb/Nb Josephson junction JJ8 (40 nm gap) measured at 20 mK. In the bottom inset the same characteristic is plotted as I versus V , where the black line is an extrapolation from high V . At $V < 0.5$ mV the excess current is clearly seen. The top inset shows the temperature dependence for JJ7 (30 nm gap) and JJ8. Right: normalized differential conductance is plotted as a function of voltage across JJ8, with $R'_N = 650 \Omega$. The enhancement of the current seen at low V is a signature of Andreev reflection. The maximum enhancement is plotted as a function of B in the inset.

in two-dimensional^{15,17} and, most relevant to the current work, in one-dimensional systems^{1,2}. Moreover, multiband nanowires are also predicted to support topological superconductivity^{18–20}.

What are the experimental signatures of Majorana particles? Majorana particles should have zero energy, and zero-energy Andreev end-modes localized at the ends of a wire can be probed in tunnelling experiments^{11,21,22}. Indeed, there are reports of a zero bias anomaly observed in topological insulator–superconductor²³ and semiconductor–superconductor^{24,25} structures. However, conductivity enhancement near zero bias can also be a signature of diverse phenomena in mesoscopic physics, such as the Kondo effect in quantum dots^{26,27} or the ‘0.7 anomaly’ in nanowires^{28,29}. Fusion of two Majorana modes produces an ordinary fermion and, uniquely to Majorana particles, modifies the periodicity of the Josephson relation from 2π (Cooper pairs) to 4π (Majorana particles)^{1,4,30–32}. In the d.c. Josephson effect, fluctuations between filled and empty Majorana modes will mask the 4π periodicity and, indeed, we observe only 2π periodicity in a d.c. SQUID (superconducting quantum interference device) configuration. In the a.c. Josephson effect, however, the 4π periodicity due to Majorana modes should be fully revealed.

In our experiments Nb/InSb/Nb Josephson junctions are fabricated lithographically from a shallow InSb quantum well. Superconductivity in InSb is induced by the proximity effect from a Nb film placed on top of the InSb nanowire. The self-aligning fabrication process which we use is described in the Supplementary Information. A pattern of multiple Josephson junctions is defined by e-beam lithography, and a 45 nm layer of Nb is deposited by d.c. sputtering on top of the InSb quantum well. An image of a Josephson junction region is shown in Fig. 1a. A weak link is formed between two 120 nm-wide and 0.6 μm -long Nb wires, with gaps ranging from 20 to 120 nm in different devices. During deposition of Nb, a thin (2–4 nm) layer of Nb is extended 70–80 nm outside the pattern, including the space inside the gaps, which can be seen as a brown halo around the Nb wire on the atomic force microscope (AFM) image. This layer is used as an etch mask to define a nanowire

in the underlying semiconductor self-aligned to the Nb wire. After the etching, a continuous $w \lesssim 290$ nm-wide InSb wire is formed under the Nb, as shown schematically in Fig. 1b. The thin Nb layer is not conducting at low temperatures, therefore the supercurrent is carried by the proximity-induced superconductivity in InSb.

The InSb wires have rectangular cross section $w \gg d$ and spin–orbit interactions are dominated by the Dresselhaus term $H_D = \gamma_D \langle k_z^2 \rangle (k_x \sigma_x - k_y \sigma_y)$, where $\langle k_z^2 \rangle = (\pi/d)^2$, $d = 20$ nm is the quantum well thickness, $\gamma_D = 760 \text{ eV \AA}^3$ for InSb, σ_i are Pauli matrices, and \hat{x} and \hat{y} are the principal crystallographic axes. We estimate $E_{so} \approx 1$ meV (refer to the Supplementary Information). The wires are oriented along the [110] crystallographic direction, and expected direction of the effective spin–orbit magnetic field \mathbf{B}_{so} is perpendicular to the current, as indicated by the green arrow on the AFM image. From the lithographical dimensions we estimate that only a few (1–3) one-dimensional subbands should be populated in InSb nanowires, however, we expect the density of states in the nanowires to be modified by the strong coupling to Nb and the actual number of filled subbands may be larger.

As devices are cooled down, a series of superconducting transitions $T_{c1} - T_{c3}$ and T_c are observed (Fig. 2). The first transition, $T_{c1} \sim 6.4$ K, is for wide areas, $T_{c2} = 5.8$ K and $T_{c3} = 1.9$ K are for the 1 and 0.12 μm -wide Nb wires, and T_c is for the Josephson junctions. From $T_c = 1.17$ K for Josephson junction JJ8 we estimate a proximity gap $\Delta \approx 180 \mu\text{eV}$ and a semiconductor–superconducting coupling $\lambda \approx 2.6\Delta$ (ref. 33). Lithographically our devices consist of two Josephson junctions in parallel, and we can measure the ratio of the critical currents in the two arms $r = I_{c1}/I_{c2}$ by measuring the magnitude of current modulation in a d.c. SQUID configuration. The ratio $r = 7.3$ for JJ7 and $r > 10$ for JJ8, indicating that conduction is dominated by a single junction. In the following analysis we will treat our devices as containing a single Josephson junction.

As seen in Fig. 2, the $V(I)$ characteristic for JJ8 measured at the base temperature of 20 mK exhibits a clear supercurrent region ($V = 0$), with an abrupt appearance of a finite voltage $\sim A$. A small hysteresis is observed for the return critical current $I_R \sim I_c$,

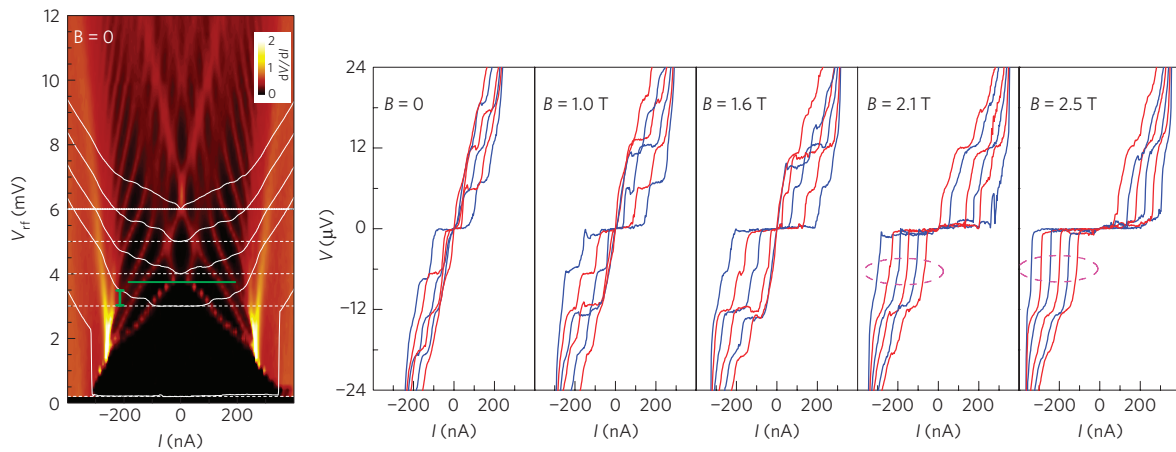


Figure 3 | a.c. Josephson effect and Shapiro steps. Left: differential resistance dV/dI (in $k\Omega$, colour scale) of JJ8 is plotted as a function of the rf amplitude V_{rf} and d.c. current I for $f_0 = 3$ GHz. The data is measured with low frequency (17 Hz) a.c. excitation $I_{a.c.} = 2$ nA at $T = 20$ mK and $B = 0$. $|V(I)|$ characteristics at $V_{rf} = 0.2, 3, 4, 5$ and 6 mV are shown as white lines; their zero is shifted vertically and is marked by dashed white lines. A horizontal green line separates low and high rf power regimes. The small vertical green bar indicates the scale of $12 \mu\text{V}$ on the $|V(I)|$ curves. Right: $V(I)$ characteristics of JJ8 in the presence of $B||I$ measured with V_{rf} between 3 and 6 mV in 0.6 mV increments. For $B < 2$ T, Shapiro steps with a height $\Delta V = h\nu_{rf}/2e = 6 \mu\text{V}$ are clearly observed. For $B > 2$ T the plateau at $6 \mu\text{V}$ disappears, as emphasized by dashed ovals, and the first step is observed at $12 \mu\text{V}$. This doubling of the first Shapiro step is a signature of the a.c. fractional Josephson effect, and is a hallmark of a topological superconductivity.

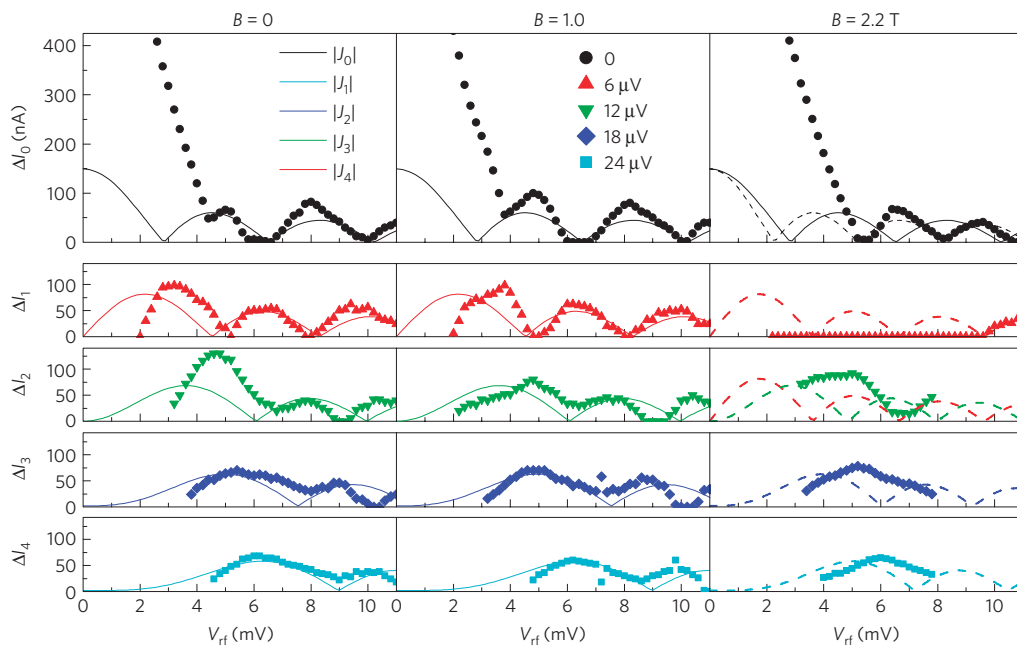


Figure 4 | Evolution of Shapiro steps with rf power. The width of the first five Shapiro steps are plotted as a function of the rf field amplitude V_{rf} . Lines are Bessel functions $A|J_n(\beta V_{rf})|$, with $\beta = 0.84 \text{ mV}^{-1}$ (solid) and $\beta = 1.04 \text{ mV}^{-1}$ (dashed).

characteristic of a resistively shunted Josephson junction in an intermediate damping regime³⁴. Indeed, we measure high leakage to the substrate, and estimate the shunting resistance $R_s \lesssim 1 \text{ k}\Omega$. The measured resistance in the normal state is $R'_N = 650 \Omega$, and the actual normal resistance of the JJ8 $R_N \approx 2\text{--}6 \text{ k}\Omega$, consistent with the number of one-dimensional channels estimated from the size of the wire. The product $R_N I_c \approx 1 \text{ mV} > 2\Delta$ indicates that JJ8 is in a clean limit (weak link length $L_{\text{eff}} < \xi, l$, where ξ is the coherence length and l is the mean free path), a proper condition for the formation of Majorana particles.

Normalized differential conductance, plotted in the right panel of Fig. 2, shows enhancement at low voltages. This excess current is a signature of Andreev reflection^{35,36}. Most important for our

measurements is that the excess current, and thus coherent electron transport, is observed at high in-plane magnetic fields up to 4 T, as shown in the the inset.

In the presence of microwave excitation, phase locking between the rf field and the Josephson supercurrent gives rise to constant-voltage Shapiro steps in the $V(I)$ characteristics at $V_n = nhf_0/q$, where h is Planck's constant, q is the charge of quasiparticles, f_0 is the microwave frequency, and $n = 0, \pm 1, \pm 2, \dots$ (ref. 37). Shapiro steps for $f_0 = 3$ GHz are shown in Fig. 3. At $B = 0$ we observe steps with a height $\Delta V = 6 \mu\text{V}$, consistent with the Cooper pair tunnelling ($q = 2e$). ΔV scales linearly with f_0 (refer to the Supplementary Information). The evolution of the steps with V_{rf} is best visualized in the dV/dI plots, where steps with $0 < n < 10$ are seen at high rf

powers. A transition from a low to high rf power regime is clearly seen in the dV/dI plot near $V_{\text{rf}} \approx 4$ mV and is marked by a green horizontal line. At high rf powers $V_{\text{rf}} > 4$ mV the evolution of the width of the Shapiro steps ΔI_n follows a Bessel function pattern as a function of power, $\Delta I_n = A|J_n(2eV_{\text{rf}}/hf_0)|$, where v_{rf} is the rf amplitude at the junction. We can find the rf power attenuation from the fit to the ΔI_0 , $v_{\text{rf}} = 5 \times 10^{-3} V_{\text{rf}}$ for $f_0 = 3$ GHz, Fig. 4. Here V_{rf} is the rf amplitude at the top of the fridge. Thus, $V_{\text{rf}} = 4$ mV corresponds to $v_{\text{rf}} = 20 \mu\text{V} \approx V_{\text{R}}/2\sqrt{2}$, where $V_{\text{R}} \approx 60 \mu\text{V}$ (see Fig. 2).

For $V_{\text{rf}} < 4$ mV the junction is in the small microwave signal regime³⁸. The linear response of a Josephson junction has a singularity at $\omega = \pm\omega_J$, where $\omega_J = 2e/\hbar V$ is the Josephson frequency, and the Josephson junction performs a parametric conversion of the external frequency. Josephson junction JJ8 is in the intermediate damping regime and the $V(I)$ characteristic is expected to become non-hysteretic in the vicinity of the first step. Indeed, we observe no hysteresis for $V_{\text{rf}} > 1.8$ mV. Although nonlinear effects can be present at high I and V_{rf} , we want to stress that the first step at the onset of the normal state is due to phase locking between the external and the Josephson frequencies, $\omega = \pm\omega_J$.

When an in-plane magnetic field $\mathbf{B}||\mathbf{I}$ is applied, Shapiro steps at $V = 6, 12$ and $18 \mu\text{V}$ are clearly visible at low fields, $B < 2$ T. Steps at 12 and $18 \mu\text{V}$ remain visible up to $B \approx 3$ T, whereas the step at $6 \mu\text{V}$ disappears above $B \approx 2$ T. The disappearance of all steps above 3 T is consistent with suppression of the excess current and Andreev reflection at high fields.

Quantitative comparison of the width of the Shapiro steps $\Delta I_n(V_{\text{rf}})$ for different B extracted from dV/dI data is plotted in Fig. 4. For $B < 2$ T steps at $0, 6, 12, 18$ and $24 \mu\text{V}$ evolve according to Bessel functions with an amplitude $A \approx 150$ nA. For $B > 2$ T the step at $6 \mu\text{V}$ vanishes at low V_{rf} , and re-appears at high $V_{\text{rf}} > 10$ mV for $B = 2.2$ T. We also observe that the low-field rf attenuation does not fit the evolution of the ΔI_0 plateau. Moreover, a minimum of the $12 \mu\text{V}$ plateau at $V_{\text{rf}} \approx 7$ meV coincides with the minimum of the $|J_1|$ Bessel function, suggesting that indeed the $12 \mu\text{V}$ plateau became the $n = 1$ Shapiro step. Evolution of plateaux at $B > 2$ T is poorly described by Bessel functions, suggesting that oscillations with different frequencies may contribute to the width of the plateaux. At high fields Majorana particles are expected to form inside the InSb wire close to the ends of the Nb wires. At these fields the supercurrent is dominated by the fusion of two Majorana particles across the gap, which amounts to the $1e$ charge transfer and leads to the doubling of the Shapiro steps. We emphasize that the doubling of the Shapiro step height is a unique signature of a topological quantum phase transition.

Theoretically it has been argued that Josephson currents with both 2π ($I_c \sin(\phi)$) and 4π ($I_M \sin(\phi/2)$) periodicity should be present in the topological state^{3,39–41}, especially in multichannel wires. However, in current-biased junctions odd steps are expected to vanish even in the presence of large supercurrents carried by the charge- $2e$ quasiparticles $I_c \gg I_M$ (ref. 42). In this case the width of even steps is expected to be defined primarily by I_c , and the coefficient A remains almost unchanged across the transition, as is observed experimentally, especially if a large number of subbands is occupied in the nanowire owing to the strong coupling to the superconductor. At high voltages across the junction we expect enhanced mixing between gapless and gapped modes, which may explain the prominence of the $18 \mu\text{V}$ and higher plateaux at $B > 2$ T.

Received 30 April 2012; accepted 20 August 2012;
published online 23 September 2012

References

- Lutchyn, R. M., Sau, J. D. & Sarma, S. D. Majorana fermions and a topological phase transition in semiconductor–superconductor heterostructures. *Phys. Rev. Lett.* **105**, 077001 (2010).
- Oreg, Y., Refael, G. & von Oppen, F. Helical liquids and Majorana bound states in quantum wires. *Phys. Rev. Lett.* **105**, 177002 (2010).
- Alicea, J., Oreg, Y., Refael, G., von Oppen, F. & Fisher, M. P. A. Non-Abelian statistics and topological quantum information processing in 1D wire networks. *Nature Phys.* **7**, 412–417 (2011).
- Kitaev, A. Y. Unpaired Majorana fermions in quantum wires. *Phys.-Usp.* **44**, 131–136 (2001).
- Kitaev, A. Y. Fault-tolerant quantum computation by anyons. *Ann. Phys.* **303**, 2–30 (2003).
- Majorana, E. Symmetrical theory of electrons and positrons. *Nuovo Cimento.* **14**, 171–184 (1937).
- Dirac, P. A. M. The quantum theory of the electron. *Proc. R. Soc. Lond. A* **117**, 610–624 (1928).
- Wilczek, F. Majorana returns. *Nature Phys.* **5**, 614–618 (2009).
- Cho, A. The sterile neutrino: Fertile concept or dead end? *Science* **334**, 304–306 (2011).
- Moore, G. & Read, N. Nonabelions in the fractional quantum Hall effect. *Nucl. Phys. B* **360**, 362–396 (1991).
- Sengupta, K., Žutić, I., Kwon, H.-J., Yakovenko, V. M. & Das Sarma, S. Midgap edge states and pairing symmetry of quasi-one-dimensional organic superconductors. *Phys. Rev. B* **63**, 144531 (2001).
- Das Sarma, S., Nayak, C. & Tewari, S. Proposal to stabilize and detect half-quantum vortices in strontium ruthenate thin films: Non-abelian braiding statistics of vortices in a $p_x + ip_y$ superconductor. *Phys. Rev. B* **73**, 220502 (2006).
- Read, N. & Green, D. Paired states of fermions in two dimensions with breaking of parity and time-reversal symmetries and the fractional quantum Hall effect. *Phys. Rev. B* **61**, 10267–10297 (2000).
- Fu, L. & Kane, C. Superconducting proximity effect and Majorana fermions at the surface of a topological insulator. *Phys. Rev. Lett.* **100**, 096407 (2008).
- Sau, J., Lutchyn, R., Tewari, S. & Das Sarma, S. Generic new platform for topological quantum computation using semiconductor heterostructures. *Phys. Rev. Lett.* **104**, 040502 (2010).
- Quay, C. *et al.* Observation of a one-dimensional spin–orbit gap in a quantum wire. *Nature Phys.* **6**, 336–339 (2010).
- Alicea, J. Majorana fermions in a tunable semiconductor device. *Phys. Rev. B* **81**, 125318 (2010).
- Lutchyn, R. M., Stanescu, T. & Sarma, S. D. Search for Majorana fermions in multiband semiconducting nanowires. *Phys. Rev. Lett.* **106**, 127001 (2011).
- Potter, A. C. & Lee, P. A. Multichannel generalization of Kitaev’s Majorana end states and a practical route to realize them in thin films. *Phys. Rev. Lett.* **105**, 227003 (2010).
- Stanescu, T., Lutchyn, R. M. & Sarma, S. D. Majorana fermions in semiconductor nanowires. *Phys. Rev. B* **84**, 144522 (2011).
- Law, K. T., Lee, P. A. & Ng, T. K. Majorana fermion induced resonant Andreev reflection. *Phys. Rev. Lett.* **103**, 237001 (2009).
- Sau, J. D., Tewari, S., Lutchyn, R., Stanescu, T. & Sarma, S. D. Non-abelian quantum order in spin–orbit-coupled semiconductors: The search for topological Majorana particles in solid state systems. *Phys. Rev. B* **82**, 214509 (2010).
- Koren, G., Kirzhner, T., Lahoud, E., Chashka, K. B. & Kanigel, A. Proximity-induced superconductivity in topological $\text{Bi}_2\text{Te}_2\text{Se}$ and Bi_2Se_3 films: Robust zero-energy bound state possibly due to Majorana fermions. *Phys. Rev. B* **84**, 224521 (2011).
- Mourik, V. *et al.* Signatures of Majorana fermions in hybrid superconductor–semiconductor nanowire devices. *Science* **336**, 1003–1007 (2012).
- Deng, M. T. *et al.* Observation of Majorana fermions in a Nb–InSb nanowire–Nb hybrid quantum device. Preprint at <http://arxiv.org/abs/1204.4130> (2012).
- Goldhaber-Gordon, D. *et al.* Kondo effect in a single-electron transistor. *Nature* **391**, 156–159 (1998).
- Rohinson, L. P., Guo, L. J., Chou, S. Y. & Tsui, D. C. Kondo-like zero-bias anomaly in electronic transport through an ultrasmall Si quantum dot. *Phys. Rev. B* **60**, R16319–R16321 (1999).
- Cronenwett, S. M. *et al.* Low-temperature fate of the 0.7 structure in a point contact: A Kondo-like correlated state in an open system. *Phys. Rev. Lett.* **88**, 226805 (2002).
- Rohinson, L., Pfeiffer, L. & West, K. Spontaneous spin polarization in quantum point contacts. *Phys. Rev. Lett.* **96**, 156602 (2006).
- Kwon, H.-J., Sengupta, K. & Yakovenko, V. Fractional a.c. Josephson effect in p- and d-wave superconductors. *Eur. Phys. J. B* **37**, 349–361 (2003).
- Fu, L. & Kane, C. L. Josephson current and noise at a superconductor/quantum-spin-Hall-insulator/superconductor junction. *Phys. Rev. B* **79**, 161408 (2009).
- Akhmerov, A. R., Dahlhaus, J. P., Hassler, F., Wimmer, M. & Beenakker, C. W. J. Quantized conductance at the Majorana phase transition in a disordered superconducting wire. *Phys. Rev. Lett.* **106**, 057001 (2011).
- Sau, J. D., Tewari, S. & Das Sarma, S. Experimental and materials considerations for the topological superconducting state in electron and hole doped semiconductors: searching for non-Abelian Majorana modes in 1D nanowires and 2D heterostructures. *Phys. Rev. B* **85**, 064512 (2012).

34. Tinkham, M. *Introduction to Superconductivity* (McGraw-Hill, 1996).
35. Andreev, A. Thermal conductivity of the intermediate state of superconductors. *Zh. Eksp. Teor. Fiz.* **46**, 1823–1828 (1964).
36. Doh, Y.-J. *et al.* Tunable supercurrent through semiconductor nanowires. *Science* **309**, 272–275 (2005).
37. Shapiro, S. Josephson currents in superconducting tunnelling: The effect of microwaves and other observations. *Phys. Rev. Lett.* **11**, 80–82 (1963).
38. Likharev, K. K. *Dynamics of Josephson Junctions and Circuits* (Gordon and Breach Science Publishing, 1984).
39. Jiang, L. *et al.* Unconventional Josephson signatures of Majorana bound states. *Phys. Rev. Lett.* **107**, 236401 (2011).
40. Pikulin, D. I. & Nazarov, Y. V. Phenomenology and dynamics of Majorana Josephson junction. Preprint at <http://arxiv.org/abs/1112.6368> (2011).
41. San-Jose, P., Prada, E. & Aguado, R. AC Josephson effect in finite-length nanowire junctions with Majorana modes. *Phys. Rev. Lett.* **108**, 257001 (2011).
42. Domínguez, F., Hassler, F. & Platero, G. On the dynamical detection of Majorana fermions in current-biased nanowires. Preprint at <http://arxiv.org/abs/1202.0642> (2012).

Acknowledgements

The work was partially supported by ARO grant W911NF-09-1-0498 (L.P.R.) and by NSF grant DMR10-05851 (J.K.F., X.L.). L.P.R. benefited from discussions with Roman Lutchyn.

Author contributions

L.P.R. conceived and performed the experiments; J.K.F. and X.L. designed and grew the heterostructures; all authors contributed to the writing of the manuscript.

Additional information

Supplementary information is available in the online version of the paper. Reprints and permissions information is available online at www.nature.com/reprints. Correspondence and requests for materials should be addressed to L.P.R.

Competing financial interests

The authors declare no competing financial interests.